TRANSVERSE MOMENTUM p_{T} SPECTRA OF STRANGE PARTICLES PRODUCTION IN DIFFERENT COLLISIONS AT $\sqrt{s_{NN}} = 2.76$, 5.02 AND 7 TeV*

Hayam Yassin†, Eman R. Abo Elyazeed‡

Physics Department, Faculty of Women for Arts, Science and Education
Ain Shams University, 11577 Cairo, Egypt

(Received February 15, 2018; accepted November 28, 2018)

We analyse the transverse momentum p_{T} spectra of strange particles K^0_{s}, Λ, and Ξ^- produced in Pb+Pb collision at $\sqrt{s_{NN}} = 2.76$ TeV, $p+\mathrm{Pb}$ collision at $\sqrt{s_{NN}} = 5.02$ TeV, and $p+p$ collision at $\sqrt{s_{NN}} = 7$ TeV in different multiplicity events measured by the CMS experiment at the Large Hadron Collider. The p_{T} spectra of strange particles are fitted by the Tsallis statistics and Boltzmann statistics, respectively. The fitting parameters are studied as a function of the multiplicity events for all systems. The Tsallis temperature (T_{Ts}), Boltzmann temperature (T_{Boltz}), and radius of the system (R) increase with both the mass and strangeness number of the particle and also increase with the multiplicity events. The non-extensive parameter (q) decreases with the increase in the mass of the particle and also decrease with the increase in the multiplicity events which means that the system tends to thermodynamic stabilization. The extracted temperatures from the two statistics for the strange particles exhibit a linear correlation.

DOI:10.5506/APhysPolB.50.37

1. Introduction

Quark–gluon plasma (QGP) was created at heavy-ion collisions at the Relativistic Heavy-Ion Collider (RHIC) and the Large Hadron Collider (LHC) [1–3]. The heavy-ion experiments seek to study strongly interacting matter under extreme conditions of high density and/or high temperatures [4]. QGP was described as the deconfinement of the colliding hadrons which rapidly expands and cools down [5]. "Hadronization" or phase transition from QGP to hadrons was found at the combination of the quarks and gluons at special temperatures defined as critical temperatures. After cooling

* Funded by SCOAP[3] under Creative Commons License, CC-BY 4.0.

† Corresponding author: hiam_hussien@women.asu.edu.eg

‡ eman.reda@women.asu.edu.eg

again, chemical freeze-out occur where the produced particles are stable [6]. One of the signatures for the creation of QGP is the enhancement of the strangeness number [7, 8]. Strange quarks are not produced into the reaction by the colliding nuclei. Therefore, any strange quarks or anti-quarks seen in experiments have been newly created from the kinetic energy of the colliding nuclei [8, 9]. Another important indication for the formation of QGP is the transverse momentum p_{T} spectra of the charged and strange particles [10] since the p_{T} spectra can give information about the chemical freeze-out — chemical potential and temperature — by utilizing many statistical models [11–17]. These statistical models describe the experimental measurements over a wide range of center-of-mass energies depending on different statistics.

The Tsallis statistics [18–23] success in fitting the experimental data [24, 25] of the transverse momentum p_{T} spectra in high-energy physics. The p_{T} spectra of all identified particles measured in $p+p$ collisions at RHIC and the LHC energies were fitted excellently by the Tsallis statistics in Refs. [26–28]. The Tsallis statistics with the transverse flow effect is used in the analysis of the p_{T} spectra of charged and strange particles in Ref. [22, 23, 29–32]. The Tsallis and Boltzmann statistics describe the p_{T} spectra of all identified particles measured in Au+Au collision and Pb+Pb collision at RHIC and LHC energies in Ref. [33]. The obtained temperatures from these previous fittings gave also some useful correlations with each other. The aim of this paper is to obtain the correlation between the Tsallis and Boltzmann temperatures from the p_{T} spectra of strange particles at different collisions and energies.

The paper is organized as follows. In Sect. 2.1, the Tsallis statistics is presented, which is used to describe the particle spectra. In Sect. 2.2, we present the Boltzmann statistics which is used to describe the particle spectra. Then we discuss the results of the description of the p_{T} spectra of strange particles at different collisions and energies by using both statistics in Sect. 3. Additionally, the dependence of the fitting parameters on the multiplicity events and particle mass is discussed in Sect. 3. Finally, in Sect. 4, the conclusion of our results is presented.

2. Transverse momentum spectra

Transverse momentum p_{T} spectra of strange particles K^0_{s}, Λ, and Ξ^- produced in Pb+Pb collision at $\sqrt{s_{NN}} = 2.76$ TeV, $p+$Pb collision at $\sqrt{s_{NN}} = 5.02$ TeV, and $p+p$ collision at $\sqrt{s_{NN}} = 7$ TeV measured by the CMS experiment will be discussed using the Tsallis and Boltzmann statistics in Sects. 2.1 and 2.2.

2.1. Tsallis statistics

The experimental measurements of the p_{T} spectra in high-energy collisions can be described by different formula of the Tsallis statistics [18, 34–36]. The total number of particles is given by

$$N = \frac{gV}{(2\pi)^3} \int_0^\infty \left[1 + (q-1)\left(\frac{E-\mu}{T_{\mathrm{Ts}}}\right)\right]^{\frac{q}{1-q}} \mathrm{d}p^3 \,, \tag{1}$$

where, T_{Ts} is the Tsallis temperature, q is the non-extensive parameter, E is the energy, p is the pressure, g is the degeneracy factor, V is the system volume, and μ is the chemical potential. The momentum distribution [37] can be obtained as

$$E\frac{\mathrm{d}^3N}{\mathrm{d}p^3} = \frac{gVE}{(2\pi)^3}\left[1 + (q-1)\left(\frac{E-\mu}{T_{\mathrm{Ts}}}\right)\right]^{\frac{q}{1-q}} . \tag{2}$$

In terms of the rapidity (y) and the transverse mass ($m_{\mathrm{T}} = \sqrt{p_{\mathrm{T}}^2 + m^2}$), energy can be written as $E = m_{\mathrm{T}} \cosh y$, so at mid-rapidity $y = 0$ and $\mu \approx 0$, Eq. (2) [38] becomes

$$\frac{1}{2\pi p_{\mathrm{T}}}\frac{\mathrm{d}^2N}{\mathrm{d}p_{\mathrm{T}}\mathrm{d}y}\bigg|_{y=0} = \frac{gVm_{\mathrm{T}}}{(2\pi)^3}\left[1 + (q-1)\left(\frac{m_{\mathrm{T}}}{T_{\mathrm{Ts}}}\right)\right]^{\frac{q}{1-q}} . \tag{3}$$

2.2. Boltzmann statistics

According to the Boltzmann statistics [39], the number of particles can be written as

$$N = \frac{gV}{(2\pi)^3} \int_0^\infty \frac{\mathrm{d}p^3}{\exp\left(\frac{E-\mu}{T_{\mathrm{Boltz}}}\right)} \,, \tag{4}$$

where T_{Boltz} is the Boltzmann temperature. The momentum distribution [39–41] can be obtained as

$$E\frac{\mathrm{d}^3N}{\mathrm{d}p^3} = \frac{gVE}{(2\pi)^3}\exp\left(\frac{\mu - E}{T_{\mathrm{Boltz}}}\right) . \tag{5}$$

The momentum distribution at mid-rapidity $y = 0$ and $\mu \approx 0$ can be given by

$$\frac{1}{2\pi p_{\mathrm{T}}}\frac{\mathrm{d}^2N}{\mathrm{d}p_{\mathrm{T}}\mathrm{d}y}\bigg|_{y=0} = \frac{gVm_{\mathrm{T}}}{(2\pi)^3}\exp\left(-\frac{m_{\mathrm{T}}}{T_{\mathrm{Boltz}}}\right) . \tag{6}$$

3. Results and discussion

The transverse momentum distributions of the strange particles K^0_s, Λ, and Ξ^-in Pb+Pb collision at $\sqrt{s_{NN}} = 2.76$ TeV, p+Pb collision at $\sqrt{s_{NN}} = 5.02$ TeV, and $p+p$ collision at $\sqrt{s_{NN}} = 7$ TeV [42] in different multiplicity intervals are fitted applying two different kinds of statistics — the Boltzmann statistics using Eq. (6) and the Tsallis statistics using Eq. (3). These are shown in Figs. 1, 2, and 3. The fitting parameters are listed in Tables I, II, and III.

Figure 1 shows the p_T spectra of the strange particles, (a) K^0_s, (b) Λ, and (c) Ξ^-, produced in Pb+Pb collision at $\sqrt{s_{NN}} = 2.76$ TeV with different multiplicity intervals. The experimental data of the CMS experiment [42] are represented by symbols. The experimental data are divided into classes based on the multiplicity intervals $N^{\text{offline}}_{\text{trk}}$ in the mid-rapidity range $|y| < 1.0$. The corresponding averaged multiplicity $\langle N_{\text{track}} \rangle = 21, 58, 92, 130, 168, 210, 253$ and 299 [43]. The solid and dashed curves are the calculated results using the Tsallis statistics (Eq. (3)) and the Boltzmann

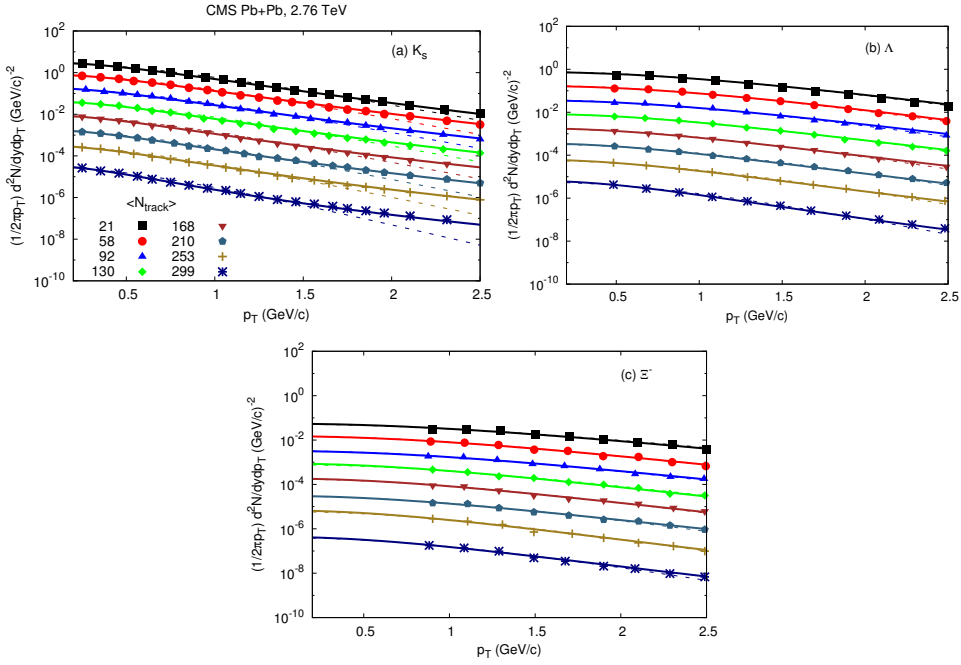

Fig. 1. Transverse momentum distributions of the strange particles K^0_s, Λ, and $\Xi^-$for Pb+Pb collision at $\sqrt{s_{NN}} = 2.76$ TeV measured in the CMS experiment (symbols) [42] are compared with calculations from the Tsallis statistics (solid curves) using Eq. (3) and with the Boltzmann statistics (dashed curves) using Eq. (6) for different multiplicity intervals.

statistics (Eq. (6)), respectively. Here, we concentrate on the smallest p_{T} region. The resulting fit parameters are given in Table I. We notice that our two results for Λ and Ξ^- particles are in a good agreement with the experimental data of Pb+Pb collisions at $\sqrt{s_{NN}} = 2.76$ TeV for all multiplicity intervals. For K^0_{s} particle, also there is a good agreement only with the results obtained from the Tsallis statistics but with the results obtained from the Boltzmann statistics, the good agreement decreases with the increase in the multiplicity classes.

Figure 2 presents the p_{T} spectra of the strange particles, (a) K^0_{s}, (b) Λ, and (c) Ξ^-, produced in p + Pb collisions at $\sqrt{s_{NN}} = 5.02$ TeV with different multiplicity intervals. The experimental data of the CMS experiment [42] are represented by symbols. The experimental data are divided into classes based on the multiplicity intervals $N^{\mathrm{offline}}_{\mathrm{trk}}$ in the mid-rapidity range $|y| < 1.0$. The corresponding averaged multiplicity $\langle N_{\mathrm{track}} \rangle = 21, 57, 89, 125, 159, 195, 236$ and 280 [43]. The solid and dashed curves are the calculated results using the Tsallis statistics (Eq. (3)) and the Boltzmann

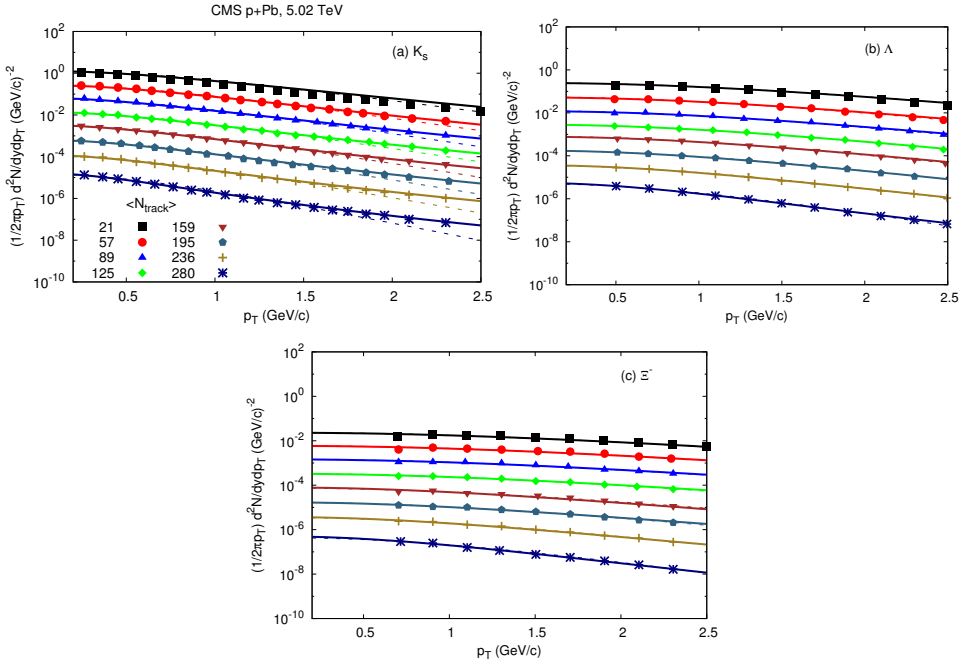

Fig. 2. Transverse momentum distributions of the strange particles K^0_{s}, Λ, and $\Xi^-$for p + Pb collision at $\sqrt{s_{NN}} = 5.02$ TeV measured in the CMS experiment (symbols) [42] are compared with calculations from the Tsallis statistics (solid curves) using Eq. (3) and with the Boltzmann statistics (dashed curves) using Eq. (6) for different multiplicity intervals.

statistics (Eq. (6)), respectively. Here, we concentrate on the smallest p_{T} region. The resulting fit parameters are given in Table II. We notice that our two results for Λ and Ξ^- particles are in a good agreement with the experimental data of $p+\mathrm{Pb}$ collisions at $\sqrt{s_{NN}} = 5.02$ TeV for all multiplicity intervals. For K^0_{s} particle, also there is a good agreement only with the results obtained from the Tsallis statistics but with the results obtained from the Boltzmann statistics, the good agreement decrease with the increasing of the multiplicity classes.

Figure 3 depicts the p_{T} spectra of the strange particles, (a) K^0_{s}, (b) Λ, and (c) Ξ^-, produced in $p+p$ collision at $\sqrt{s_{NN}} = 7$ TeV with different multiplicity intervals. The experimental data of the CMS experiment [42] are represented by symbols. The experimental data are divided into classes based on the multiplicity intervals $N^{\mathrm{offline}}_{\mathrm{trk}}$ in the mid-rapidity range $|y| < 1.0$. The corresponding averaged multiplicity $\langle N_{\mathrm{track}} \rangle = 14, 50, 79, 111, 135$ and 158 [43]. The solid and dashed curves are the calculated results using the Tsallis statistics (Eq. (3)) and the Boltzmann statistics (Eq. (6)),

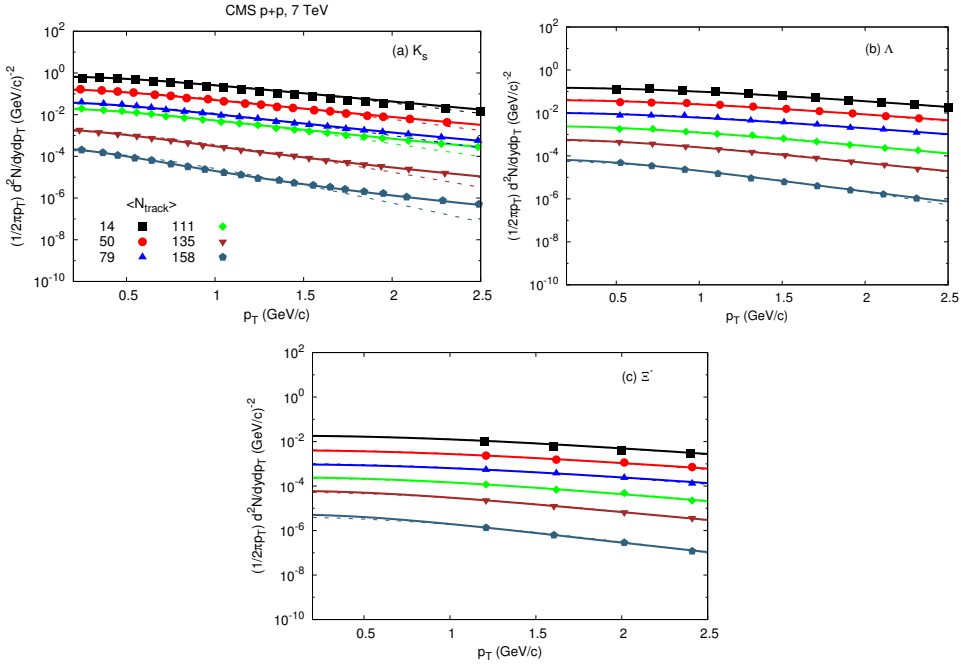

Fig. 3. Transverse momentum distributions of the strange particles K^0_{s}, Λ, and $\Xi^-$for $p+p$ collision at $\sqrt{s_{NN}} = 7$ TeV measured in the CMS experiment (symbols) [42] are compared with calculations from the Tsallis statistics (solid curves) using Eq. (3) and with the Boltzmann statistics (dashed curves) using Eq. (6) for different multiplicity intervals.

respectively. Here, we concentrate on the smallest p_{T} region. The resulting fit parameters are given in Table III. We notice that our two results for Λ and Ξ^- particles are in a good agreement with the experimental data of $p+p$ collisions at $\sqrt{s_{NN}} = 7$ TeV for all multiplicity intervals. For K^0_{s} particle, also there is a good agreement only with the results obtained from the Tsallis statistics but with the results obtained from the Boltzmann statistics, the good agreement decrease with the increase in the multiplicity intervals.

As seen from Tables I, II, and III, the value of χ^2/d.o.f. is small which represents the good quality of the fitting. Especially, the Tsallis statistics gives excellent agreement with the experimental measurements for all multiplicity classes. In addition, the fitting results of the Tsallis statistics are better than those of the Boltzmann statistics, especially at high range of p_{T}.

Furthermore, we have extracted the fitting parameters: the non-extensive parameter q, the Tsallis temperature parameter T_{Ts}, and the Boltzmann temperature parameter T_{Boltz} which inform us about the variations between the Tsallis and Boltzmann statistics. There is also another fitting parameter known as the radius R as we assume that the geometry of the fireball is spherical, so $R = (3V/4\pi)^{1/3}$ which signifies the dimension of the system and is related to the normalization in the statistical distribution function used in describing the particle yield or spectra [44].

Figure 4 (a)–(c) depicts the fitting parameter q for the strange particles K^0_{s}, Λ, and Ξ^-as a function of $\langle N_{\mathrm{track}}\rangle$ produced in the Pb+Pb, $p+$Pb and $p+p$ collisions at $\sqrt{s_{NN}} = 2.76, 5.02$, and 7 TeV, respectively. Results are obtained using the Tsallis statistics and modified Tsallis statistics [30]. The value of q (our calculations) decreases with the increasing of both the particle mass and strangeness number and also with the increasing in the multiplicity events for all systems. Our results differ from the ones modified in the effect of multiplicity on the non-extensivity parameter. This decreasing indicates that the system tend to be in equilibrium (thermodynamically).

Figure 5 (a)–(c) shows the fitting parameter R for the strange particles K^0_{s}, Λ, and Ξ^-as a function of $\langle N_{\mathrm{track}}\rangle$ produced in the Pb+Pb, $p+$Pb and $p+p$ collisions at $\sqrt{s_{NN}} = 2.76, 5.02$, and 7 TeV, respectively. The value of R increases with the increasing in the multiplicity classes but decreases with the increase in the particle mass. So the volume of the system increases with the increase in the multiplicity events as expected.

TABLE I

Parameters deduced for the fitting of Tsallis and Boltzmann transverse momentum distributions at different multiplicity intervals for Pb+Pb collision at $\sqrt{s_{NN}} = 2.76$ TeV, see Fig. 1.

Particle	$\langle N_{\rm track}\rangle$	$T_{\rm Ts}$ [MeV]	q	R [fm]	χ^2/d.o.f.	$T_{\rm Boltz}$ [MeV]	R [fm]	χ^2/d.o.f.
K^0_s	21	87.169 ± 0.105	1.15 ± 0.001	0.154 ± 0.026	0.023	198.808 ± 1.672	0.07 ± 0.021	0.13
	58	133.113 ± 0.378	1.1224 ± 0.003	0.211 ± 0.044	0.047	220.873 ± 1.47	0.136 ± 0.036	0.1
	92	139.857 ± 0.131	1.1189 ± 0.001	0.358 ± 0.052	0.015	228.78 ± 1.46	0.236 ± 0.062	0.09
	130	147.611 ± 0.283	1.1158 ± 0.002	0.589 ± 0.107	0.03	238.526 ± 1.749	0.394 ± 0.107	0.1
	168	165.663 ± 0.418	1.1017 ± 0.003	0.894 ± 0.175	0.038	248.365 ± 1.7	0.642 ± 0.169	0.091
	210	170.876 ± 0.345	1.1007 ± 0.003	1.421 ± 0.257	0.03	248.671 ± 1.624	1.051 ± 0.273	0.087
	253	181.643 ± 0.294	1.0941 ± 0.002	2.226 ± 0.371	0.023	249.084 ± 1.053	1.741 ± 0.391	0.056
	299	188.54 ± 0.499	1.079 ± 0.004	3.381 ± 0.622	0.031	256.769 ± 2.215	2.65 ± 0.737	0.108
Λ	21	91.274 ± 0.084	1.11 ± 0.0003	0.193 ± 0.034	0.056	249.745 ± 1.111	0.046 ± 0.013	0.233
	58	160.973 ± 0.093	1.09 ± 0.0003	0.166 ± 0.024	0.03	289.72 ± 0.944	0.082 ± 0.02	0.15
	92	187.226 ± 0.27	1.08 ± 0.001	0.242 ± 0.046	0.07	304.703 ± 1.244	0.137 ± 0.036	0.181
	130	229.993 ± 0.164	1.064 ± 0.001	0.321 ± 0.047	0.032	309.954 ± 0.359	0.235 ± 0.04	0.05
	168	274.28 ± 0.412	1.0429 ± 0.001	0.441 ± 0.082	0.064	329.929 ± 0.511	0.366 ± 0.068	0.064
	210	322.756 ± 1.085	1.0245 ± 0.003	0.605 ± 0.143	0.132	335.32 ± 1.454	0.597 ± 0.156	0.178
	253	343.331 ± 1.146	1.0086 ± 0.003	0.957 ± 0.179	0.13	340.261 ± 1.479	0.982 ± 0.255	0.176
	299	362.632 ± 0.633	1.0067 ± 0.002	1.488 ± 0.279	0.066	360.228 ± 0.887	1.515 ± 0.321	0.095
Ξ^-	21	156.108 ± 0.513	1.09 ± 0.001	0.042 ± 0.011	0.246	290.041 ± 1.119	0.019 ± 0.165	0.284
	58	188.975 ± 0.719	1.07 ± 0.001	0.081 ± 0.023	0.282	309.878 ± 1.633	0.042 ± 0.12	0.367
	92	257.487 ± 1.258	1.0599 ± 0.003	0.085 ± 0.025	0.312	340.112 ± 2.124	0.063 ± 0.075	0.402
	130	265.875 ± 1.243	1.052 ± 0.002	0.151 ± 0.043	0.3	349.961 ± 2.211	0.11 ± 0.047	0.394
	168	286.238 ± 0.784	1.0441 ± 0.002	0.231 ± 0.055	0.172	379.967 ± 1.907	0.164 ± 0.035	0.292
	210	365.428 ± 1.569	1.0248 ± 0.003	0.27 ± 0.072	0.238	390.23 ± 2.162	0.257 ± 0.02	0.314
	253	377.162 ± 1.579	1.0168 ± 0.003	0.437 ± 0.116	0.232	400.073 ± 2.165	0.414 ± 0.013	0.301
	299	425.295 ± 2.719	1.0152 ± 0.005	0.595 ± 0.176	0.322	470.406 ± 3.561	0.533 ± 0.005	0.368

TABLE II

Parameters deduced for the fitting of Tsallis and Boltzmann transverse momentum distributions at different multiplicity intervals for $p+$Pb collision collision at $\sqrt{s_{NN}} = 5.02$ TeV, see Fig. 2.

Particle	$\langle N_{\rm track}\rangle$	$T_{\rm Ts}$ [MeV]	q	R [fm]	χ^2/d.o.f.	$T_{\rm Boltz}$ [MeV]	R[fm]	χ^2/d.o.f.
$K^0_{\rm s}$	21	133.898 ± 0.295	1.1307 ± 0.002	0.077 ± 0.015	0.035	228.653 ± 1.589	0.049 ± 0.013	0.098
	57	179.121 ± 0.646	1.1147 ± 0.005	0.118 ± 0.026	0.051	256.887 ± 1.525	0.09 ± 0.023	0.078
	89	199.756 ± 0.687	1.1083 ± 0.005	0.19 ± 0.04	0.046	269.206 ± 1.133	0.153 ± 0.034	0.054
	125	206.332 ± 0.489	1.1047 ± 0.004	0.32 ± 0.059	0.031	278.893 ± 1.433	0.258 ± 0.06	0.064
	159	218.697 ± 0.833	1.1021 ± 0.006	0.497 ± 0.106	0.048	288.99 ± 1.548	0.409 ± 0.096	0.065
	195	226.848 ± 1.085	1.1005 ± 0.008	0.81 ± 0.185	0.06	294.12 ± 1.769	0.678 ± 0.165	0.072
	236	255.94 ± 1.87	1.0787 ± 0.013	1.205 ± 0.312	0.087	309.36 ± 2.499	1.063 ± 0.282	0.093
	280	293.332 ± 1.425	1.0676 ± 0.009	1.869 ± 0.419	0.056	334.762 ± 1.591	1.721 ± 0.382	0.055
Λ	21	172.072 ± 0.124	1.09 ± 0.0004	0.067 ± 0.01	0.036	299.715 ± 0.865	0.035 ± 0.008	0.13
	57	297.482 ± 0.386	1.0499 ± 0.001	0.065 ± 0.011	0.052	369.708 ± 0.797	0.053 ± 0.011	0.083
	89	373.144 ± 0.253	1.0249 ± 0.001	0.089 ± 0.012	0.024	409.837 ± 0.47	0.082 ± 0.013	0.04
	125	436.177 ± 1.142	1.0091 ± 0.003	0.127 ± 0.026	0.085	430.532 ± 1.625	0.131 ± 0.031	0.127
	159	453.51 ± 0.919	1.0065 ± 0.003	0.19 ± 0.035	0.064	460.097 ± 1.122	0.188 ± 0.037	0.077
	195	482.8 ± 2.922	1.0047 ± 0.008	0.292 ± 0.077	0.183	470.728 ± 3.661	0.302 ± 0.087	0.243
	236	501.749 ± 2.302	1.0034 ± 0.007	0.465 ± 0.111	0.135	480.908 ± 2.991	0.487 ± 0.13	0.192
	280	531.914 ± 2.423	1.0012 ± 0.007	0.747 ± 0.176	0.131	535.578 ± 2.905	0.744 ± 0.186	0.157
Ξ^-	21	192.967 ± 0.508	1.083 ± 0.001	0.031 ± 0.008	0.176	339.7 ± 1.556	0.016 ± 0.009	0.277
	57	301.869 ± 1.753	1.0711 ± 0.004	0.034 ± 0.01	0.306	420.171 ± 1.799	0.024 ± 0.006	0.217
	89	396.942 ± 2.066	1.0684 ± 0.005	0.042 ± 0.011	0.232	480.405 ± 2.054	0.036 ± 0.019	0.194
	125	423.094 ± 4.797	1.049 ± 0.013	0.067 ± 0.023	0.547	531.027 ± 4.793	0.054 ± 0.017	0.38
	159	568.425 ± 26.71	1.0287 ± 0.01	0.084 ± 0.022	0.236	580.505 ± 3.308	0.083 ± 0.022	0.222
	195	610.815 ± 6.597	1.0219 ± 0.02	0.131 ± 0.041	0.382	630.846 ± 6.12	0.128 ± 0.039	0.317
	236	642.08 ± 7.933	1.0189 ± 0.019	0.202 ± 0.066	0.437	662.482 ± 9.601	0.198 ± 0.069	0.051
	280	660.022 ± 10.78	1.0139 ± 0.04	0.311 ± 0.111	0.558	672.726 ± 9.541	0.308 ± 0.104	0.488

TABLE III

Parameters deduced for the fitting of Tsallis and Boltzmann transverse momentum distributions at different multiplicity intervals for $p+p$ collision at $\sqrt{s_{NN}} = 7$ TeV, see Fig. 3.

Particle	$\langle N_{\rm track} \rangle$	$T_{\rm Ts}$ [MeV]	q	R [fm]	χ^2/d.o.f.	$T_{\rm Boltz}$ [MeV]	R [fm]	χ^2/d.o.f.
$K^0_{\rm s}$	14	91.407 ± 0.129	1.154 ± 0.001	0.282 ± 0.049	0.026	213.472 ± 2.176	0.126 ± 0.04	0.159
	50	155.351 ± 0.397	1.1328 ± 0.003	0.337 ± 0.066	0.037	258.135 ± 2.336	0.225 ± 0.065	0.123
	79	234.716 ± 1.78	1.1047 ± 0.013	0.536 ± 0.142	0.093	294.827 ± 2.402	0.463 ± 0.125	0.097
	111	235.749 ± 1.784	1.1028 ± 0.013	0.673 ± 0.178	0.093	308.689 ± 2.798	0.561 ± 0.155	0.105
	135	252.973 ± 1.445	1.1082 ± 0.011	1.042 ± 0.247	0.067	333.049 ± 2.631	0.869 ± 0.226	0.088
	158	313.052 ± 1.92	1.0691 ± 0.011	1.472 ± 0.355	0.07	359.903 ± 2.047	1.355 ± 0.317	0.064
Λ	14	152.631 ± 0.284	1.0945 ± 0.0008	0.183 ± 0.039	0.094	289.682 ± 1.218	0.082 ± 0.023	0.209
	50	259.374 ± 0.211	1.08 ± 0.001	0.186 ± 0.028	0.033	379.636 ± 1.303	0.127 ± 0.03	0.136
	79	321.4 ± 1.805	1.0714 ± 0.005	0.241 ± 0.066	0.202	419.733 ± 2.041	0.193 ± 0.05	0.178
	111	413.873 ± 3.627	1.0688 ± 0.011	0.309 ± 0.093	0.268	490.01 ± 3.286	0.278 ± 0.077	0.216
	135	459.049 ± 2.757	1.0519 ± 0.008	0.452 ± 0.118	0.176	500.921 ± 2.72	0.434 ± 0.113	0.175
	158	501.352 ± 3.193	1.0336 ± 0.009	0.661 ± 0.173	0.18	541.774 ± 4.08	0.627 ± 0.174	0.213
Ξ^-	14	155.92 ± 0.093	1.099 ± 0.0002	0.093 ± 0.014	0.045	339.888 ± 0.995	0.032 ± 0.008	0.203
	50	274.655 ± 0.151	1.076 ± 0.0003	0.096 ± 0.013	0.034	409.925 ± 1.02	0.062 ± 0.014	0.146
	79	419.894 ± 1.824	1.0299 ± 0.003	0.098 ± 0.026	0.229	489.854 ± 3.369	0.084 ± 0.025	0.345
	111	516.464 ± 1.844	1.028 ± 0.004	0.128 ± 0.03	0.159	520.321 ± 2.446	0.131 ± 0.034	0.225
	135	528.961 ± 2.024	1.027 ± 0.004	0.204 ± 0.048	0.164	540.85 ± 4.672	0.205 ± 0.065	0.403
	158	539.162 ± 3.965	1.0204 ± 0.008	0.333 ± 0.099	0.326	554.286 ± 5.984	0.329 ± 0.111	0.485

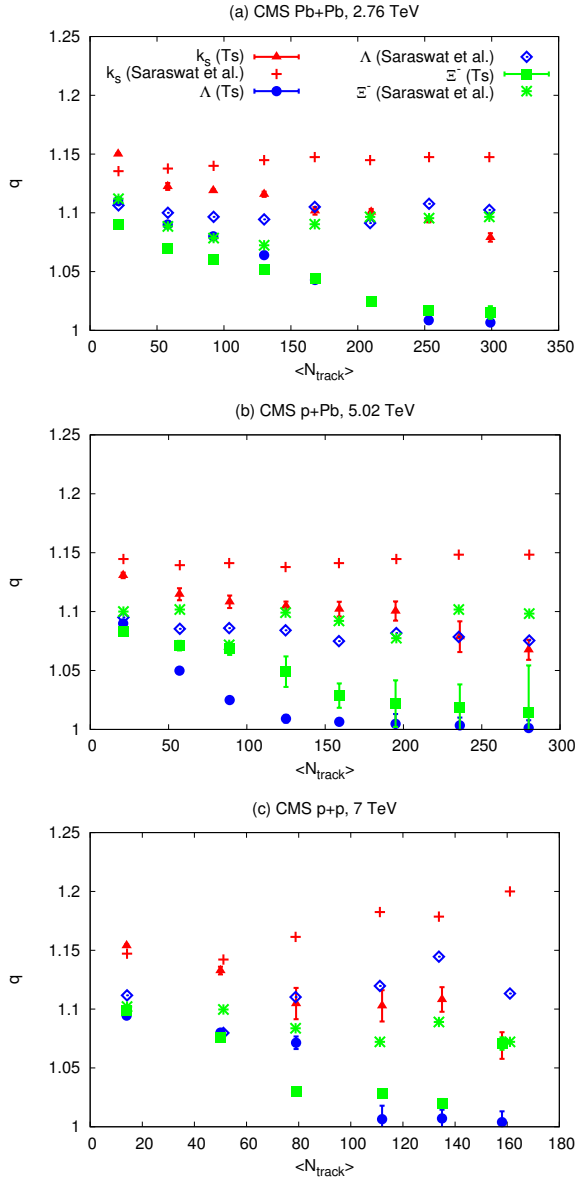

Fig. 4. The fitting parameter q as a function of the event multiplicity $\langle N_{\rm track}\rangle$ for the strange particles $K^0_{\rm s}$, Λ, and Ξ^-fitted using the Tsallis and Boltzmann statistics for (a) Pb+Pb collision at $\sqrt{s_{NN}} = 2.76$ TeV, (b) $p + \mathrm{Pb}$ collision at $\sqrt{s_{NN}} = 5.02$ TeV, and (c) $p + p$ collision at $\sqrt{s_{NN}} = 7$ TeV.

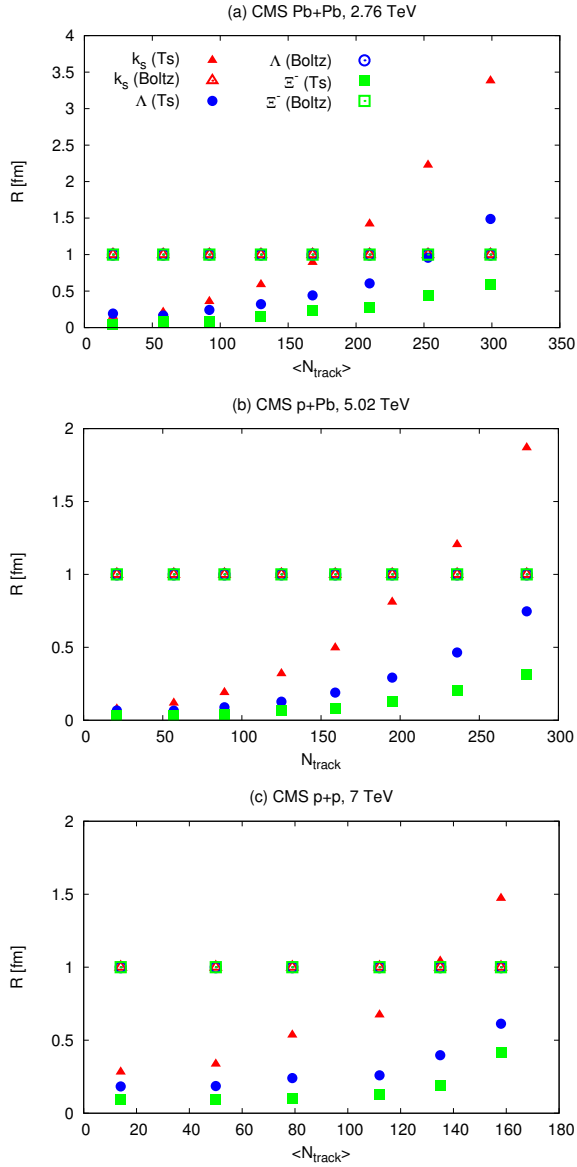

Fig. 5. The fitting parameter R as a function of the event multiplicity $\langle N_{\rm track}\rangle$ for the strange particles $K^0_{\rm s}$, Λ, and Ξ^-fitted using the Tsallis and Boltzmann statistics for (a) Pb+Pb collision at $\sqrt{s_{NN}} = 2.76$ TeV, (b) $p+$Pb collision at $\sqrt{s_{NN}} = 5.02$ TeV, and (c) $p+p$ collision at $\sqrt{s_{NN}} = 7$ TeV.

We compare our obtained values of R with Hanbury-Brown–Twiss (HBT) radii [45–47] at different center-of-mass energies $\sqrt{s_{NN}}$ as shown in Fig. 6. The fitting parameter R for the strange particles K^0_s, Λ, and $\Xi^-$and from HBT radii was obtained at most central collisions and also at mid-rapidity (for details on HBT radius parameters, see Refs. [48–52]). The obtained values of R show the same behaviour as R from HBT, especially R_{long}.

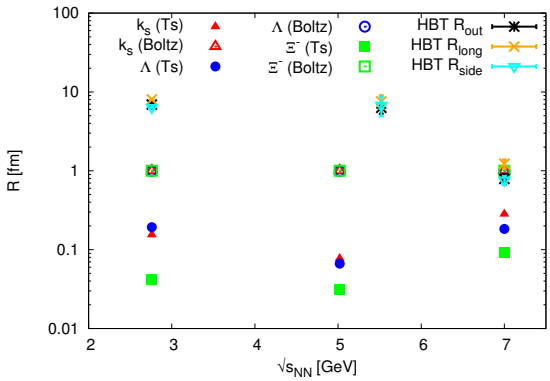

Fig. 6. The parameter R as a function of the center-of-mass energy $\sqrt{s_{NN}}$ for the obtained strange particles K^0_s, Λ, and Ξ^-fitted using the Tsallis and Boltzmann statistics and values of HBT radii ($R_{\text{out}}, R_{\text{long}}, R_{\text{side}}$) [45–47].

Figure 7 (a)–(c) depicts the fitting parameter T for the strange particles K^0_s, Λ, and Ξ^-as a function of $\langle N_{\text{track}}\rangle$ produced in the Pb+Pb, $p+$Pb and $p+p$ collisions at $\sqrt{s_{NN}} = 2.76, 5.02$, and 7 TeV, respectively. The values of both temperatures (Tsallis and Boltzmann) increase with the increase in both the particle mass and the strangeness number and also with the multiplicity classes for all systems. The direct relationship between the temperature and the strangeness number of hadrons is unlike the known behaviour obtained previously in extensive models (particle yields and ratios) [53, 54], so we will work on the confirmation of the behaviour of this dependence in extensive and non-extensive particle yields and ratios in future work. Our calculations are compared with the modified Tsallis results [30] and agree with each other. The freeze-out of particles with large mass occurs earlier than that of small mass. When the volume is small, the particle with large mass freeze out early [4]. Also, the Boltzmann temperature is always greater than the Tsallis one which is independent of the type of particles or systems, so $T_{\text{Boltz}} > T_{\text{Ts}}$.

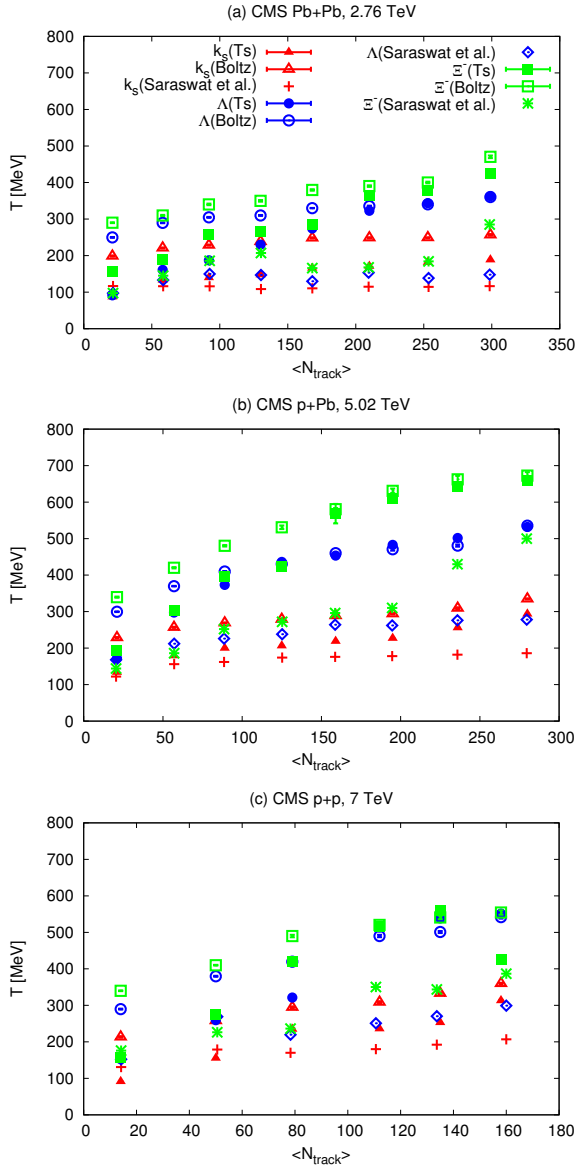

Fig. 7. The fitting parameter T as a function of the event multiplicity $\langle N_{\rm track}\rangle$ for the strange particles $K^0_{\rm s}$, Λ, and Ξ^-fitted using the Tsallis and Boltzmann statistics for (a) Pb+Pb collision at $\sqrt{s_{NN}} = 2.76$ TeV, (b) $p + {\rm Pb}$ collision at $\sqrt{s_{NN}} = 5.02$ TeV, and (c) $p + p$ collision at $\sqrt{s_{NN}} = 7$ TeV.

Figure 8 shows the relation between $T_{\rm Ts}$ and $T_{\rm Boltz}$, where all values of temperatures obtained from Figs. 1, 2, and 3 and listed in Tables I, II, and III are given by symbols. The fitted result for all strange particles at different collisions is given by the solid line which is described by

$$T_{\rm Ts} = a \;\; T_{\rm Boltz} + b\,,$$

where $a = 1.2465 \pm 0.0138$ and $b = -160.499 \pm 5.386$ are constants with $\chi^2/\text{d.o.f.} = 0.0528$. However, these values are different for different particles, so this linear relation is the same for all particles but the values of constants are different depending on the mass of the particle. The dependence of the constants on the particle type is listed in Table IV.

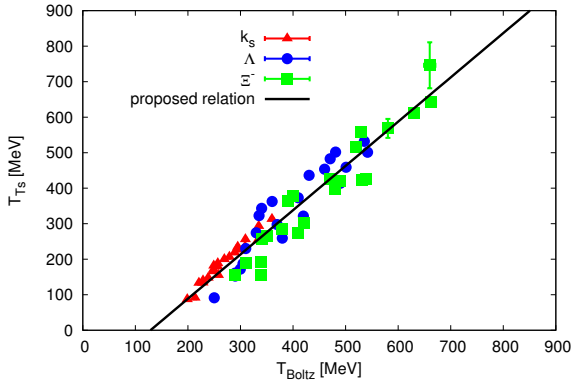

Fig. 8. The Tsallis temperature $T_{\rm Ts}$ as a function of the Boltzmann temperature $T_{\rm Boltz}$. All values of temperatures obtained from Figs. 1, 2, and 3 listed in Tables I, II, and III are given by symbols. The solid line represents the fitted result given by Eq. (3).

TABLE IV

Constants values deduced from the fitting of linear relation between the Tsallis and Boltzmann temperatures, see Fig. 8.

Particle	a	b	χ^2/d.o.f.
$K^0_{\rm s}$	(1.3714 ± 0.0092)	(-177.514 ± 2.503)	0.0319
Λ	(1.3856 ± 0.0255)	(-209.84 ± 10.2)	0.0876
Ξ^-	(1.39513 ± 0.0212)	(-249.213 ± 9.963)	0.0722

As can be seen from Table IV, the value of constant a increases with the increase of the particle mass but the constant b is inversely proportional to the particle mass. A similar linear relation between T_{Ts} and T_{Boltz} for charged (but not strange) particles at various collisions was found in Ref. [33]. The values of constants a and b for the charged non-strange particles confirm our concept about the dependence of the constants on the particle mass.

Therefore, we can find a direct relation between any temperature and the Boltzmann temperature, and consider the Boltzmann temperature as the reference for all other temperatures [33]. However, the Boltzmann statistics fails to fit some experimental transverse momentum spectra especially at high-p_{T} region as a result of using the simplest form of the Boltzmann statistics [16, 33, 41, 55]. On the contrary, the Tsallis statistics succeeded in depicting all experimental transverse momentum spectra used in the present work and also at high region of p_{T} [30, 33, 35, 56–61]. We also compare our Tsallis results with the modified Tsallis one [30] (with a radial flow). Our Tsallis temperatures are greater than modified ones [30]. The reason for this increasing gets from neglecting the effect of the radial flow. We neglect this parameter as a result of the considered low range of transverse momentum [33].

4. Conclusion

We analysed the transverse momentum p_{T} spectra of the strange particles K^0_{s}, Λ, and Ξ^-in different multiplicity events produced in Pb+Pb collision at $\sqrt{s_{NN}} = 2.76$ TeV, $p+\mathrm{Pb}$ collision at $\sqrt{s_{NN}} = 5.02$ TeV, and $p+p$ collision at $\sqrt{s_{NN}} = 7$ TeV using the Tsallis and Boltzmann statistics. In nearly all cases, our Tsallis and Boltzmann results are in an excellent agreement with the experimental data of the CMS Collaboration at the LHC. Except for K^0_{s}, the goodness of our Boltzmann results decreases with the increase in the multiplicity events.

In all studied collisions, for all particles in different multiplicity events, the Tsallis T_{Ts} and Boltzmann T_{Boltz} temperature values increase with the increase in the mass of the mentioned particle. Moreover, there is a direct relationship between the values of the temperatures and the multiplicity events. We observe that $T_{\mathrm{Ts}} < T_{\mathrm{Boltz}}$, the value of q is inversely proportional with the multiplicity events in all studied systems, and the value of R in both statistics increases with the increase in the multiplicity events. There is also the direct dependence of the multiplicity on the size of the volume of the system.

There is a linear relation between the Tsallis temperature T_{Ts} and the Boltzmann temperature T_{Boltz}. We have $T_{\mathrm{Ts}} = (1.3714 \pm 0.0092)\ T_{\mathrm{Boltz}} + (-177.514 \pm 2.503)$ for K^0_{s}, $T_{\mathrm{Ts}} = (1.3856 \pm 0.0255)\ T_{\mathrm{Boltz}} + (-209.84 \pm$

10.2) for Λ, and $T_{\rm Ts} = (1.39513 \pm 0.0212)\ T_{\rm Boltz} + (-249.213 \pm 9.963)$ for Ξ^-.Besides, we have $T_{\rm Ts} = (1.2465 \pm 0.0138)\ T_{\rm Boltz} + (-160.499 \pm 5.386)$ for all studied strange particles. In all cases, $T_{\rm Ts} < T_{\rm Boltz}$ as the Boltzmann temperature is considered as the base for all other temperatures, and both values of temperatures increase with the increase in the particle mass at vanishing chemical potential.

REFERENCES

[1] J.D. Bjorken, *Phys. Rev. D* **27**, 140 (1983).

[2] T. Ullrich, B. Wyslouch, J.W. Harris, *Nucl. Phys. A* **904–905**, 1c (2013).

[3] M. Gyulassy, L. McLerran, *Nucl. Phys. A* **750**, 30 (2005).

[4] A. Khuntia, S. Tripathy, R. Sahoo, J. Cleymans, *Eur. Phys. J. A* **53**, 103 (2017).

[5] S. Ahmad *et al.*, *Adv. High Energy Phys.* **2013**, 836071 (2013).

[6] A. Tawfik, *Int. J. Mod. Phys. A* **29**, 1430021 (2014).

[7] J. Letessier, J. Rafelski, A. Tounsi, *Phys. Rev. C* **50**, 406 (1994).

[8] J. Adam *et al.* [ALICE Collaboration], *Nature Phys.* **13**, 535 (2017).

[9] J. Rafelski, B. Müller, *Phys. Rev. Lett.* **48**, 1066 (1982) [*Erratum ibid.* **56**, 2334 (1986)].

[10] H.-C. Song *et al.*, *Phys. Rev. Lett.* **106**, 192301 (2011) [*Erratum ibid.* **109**, 139904 (2012)].

[11] J. Adams *et al.* [STAR Collaboration], *Phys. Rev. Lett.* **92**, 112301 (2004).

[12] F. Becattini, *J. Phys. Conf. Ser.* **5**, 175 (2005).

[13] A.H. Mueller, *Nucl. Phys. B* **415**, 373 (1994).

[14] A.H. Mueller, B. Patel, *Nucl. Phys. B* **425**, 471 (1994).

[15] A.H. Mueller, *Nucl. Phys. B* **437**, 107 (1995).

[16] E. Schnedermann, J. Sollfrank, U.W. Heinz, *Phys. Rev. C* **48**, 2462 (1993).

[17] A.N. Tawfik, H. Yassin, E.R. Abo Elyazeed, *Chin. Phys. C* **41**, 053107 (2017).

[18] C. Tsallis, *J. Statist. Phys.* **52**, 479 (1988).

[19] T.S. Biró, G. Purcsel, K. Ürmössy, *Eur. Phys. J. A* **40**, 325 (2009).

[20] T. Bhattacharyya *et al.*, *Eur. Phys. J. A* **52**, 30 (2016).

[21] H. Zheng, L. Zhu, *Adv. High Energy Phys.* **2015**, 180491 (2015).

[22] Z. Tang *et al.*, *Phys. Rev. C* **79**, 051901 (2009).

[23] B. De, *Eur. Phys. J. A* **50**, 138 (2014).

[24] A. Adare *et al.* [PHENIX Collaboration], *Phys. Rev. C* **83**, 064903 (2011).

[25] V. Khachatryan *et al.* [CMS Collaboration], *J. High Energy Phys.* **1105**, 064 (2011).

[26] P.K. Khandai, P. Sett, P. Shukla, V. Singh, *Int. J. Mod. Phys. A* **28**, 1350066 (2013).

[27] A. Adare *et al.* [PHENIX Collaboration], *Phys. Rev. D* **83**, 052004 (2011).
[28] P. Sett, P. Shukla, *Adv. High Energy Phys.* **2014**, 896037 (2014).
[29] P.K. Khandai, P. Sett, P. Shukla, V. Singh, *J. Phys. G* **41**, 025105 (2014).
[30] K. Saraswat, P. Shukla, V. Kumar, V. Singh, *Eur. Phys. J. A* **53**, 5 (2017).
[31] J. Cleymans, D. Worku, *J. Phys. G* **39**, 025006 (2012).
[32] P. Sett, P. Shukla, *Int. J. Mod. Phys. E* **24**, 1550046 (2015).
[33] Y.-Q. Gao, F.-H. Liu, *Indian J. Phys.* **90**, 319 (2016).
[34] C. Tsallis, R.S. Mendes, A.R. Plastino, *Physica A* **261**, 534 (1998).
[35] J. Cleymans, D. Worku, *Eur. Phys. J. A* **48**, 160 (2012).
[36] J. Cleymans, M.D. Azmi, *Eur. Phys. J. C* **75**, 430 (2015).
[37] J. Cleymans, M.D. Azmi, *J. Phys. Conf. Ser.* **668**, 012050 (2016).
[38] B.C. Li *et al.*, *Adv. High Energy Phys.* **2015**, 741816 (2015).
[39] P.-Z. Ning, L. Li, D.-F. Min, *Foundation of Nuclear Physics: Nucleons and Nuclei*, Higher Education Press, Beijing, China, 2003.
[40] C.D. Dermer, *Astrophys. J.* **280**, 328 (1984).
[41] C.-R. Meng, *Chin. Phys. Lett.* **26**, 102501 (2009).
[42] V. Khachatryan *et al.* [CMS Collaboration], *Phys. Lett. B* **768**, 103 (2017).
[43] S. Chatrchyan *et al.* [CMS Collaboration], *Phys. Lett. B* **724**, 213 (2013).
[44] J. Cleymans *et al.*, *Phys. Lett. B* **723**, 351 (2013).
[45] K. Aamodt *et al.* [ALICE Collaboration], *Phys. Lett. B* **696**, 328 (2011).
[46] V.A. Okorokov, *Adv. High Energy Phys.* **2015**, 790646 (2015).
[47] A. Bialas, W. Florkowski, K. Zalewski, *J. Phys. G* **42**, 045001 (2015).
[48] A.N. Makhlin, Yu.M. Sinyukov, *Z. Phys. C* **39**, 69 (1988).
[49] D. Boal, C.G. Gelbke, B. Jennings, *Rev. Mod. Phys.* **62**, 553 (1990).
[50] U. Mayer, E. Schnedermann, U. Heinz, *Phys. Lett. B* **294**, 69 (1992).
[51] S.V. Akkelin, Yu.M. Sinyukov, *Phys. Lett. B* **356**, 525 (1995).
[52] S. Chapman, P. Scotto, U. Heinz, *Phys. Rev. Lett.* **74**, 4400 (1995).
[53] P. Castorina, H. Satz, *Adv. High Energy Phys.* **2014**, 376982 (2014).
[54] A.N. Tawfik, H. Yassin, E.R.A. Elyazeed, *Int. J. Mod. Phys. E* **26**, 1750001 (2017).
[55] H. Zhao, F.-H. Liu, *Adv. High Energy Phys.* **2014**, 742193 (2014).
[56] C.-Y. Wong, G. Wilk, *Acta Phys. Pol. B* **43**, 2047 (2012).
[57] K. Urmosy, G.G. Barnaföldi, T.S. Biró, *Phys. Lett. B* **718**, 125 (2012).
[58] G. Wilk, Z. Włodarczyk, *Eur. Phys. J. A* **48**, 161 (2012).
[59] L. Marques, J. Cleymans, A. Deppman, *Phys. Rev. D* **91**, 054025 (2015).
[60] L. Marques, E. Andrade-II, A. Deppman, *Phys. Rev. D* **87**, 114022 (2013).
[61] M.D. Azmi, J. Cleymans, *J. Phys. G* **41**, 065001 (2014).